Global phase diagram of perovskite manganites in the plane of quenched disorder versus one-electron bandwidth

Y. Tomioka[1] and Y. Tokura[1,2,3]
[1]*Correlated Electron Research Center (CERC), National Institute of Advanced Industrial Science and Technology (AIST), Tsukuba 305-8562, Japan*
[2]*Spin Superstructure Project, ERATO, Japan Science and Technology Corporation (JST), Tsukuba 305-8562, Japan*
[3]*Department of Applied Physics, University of Tokyo, Tokyo 113-8656, Japan*
(Received 1 March 2004; published 29 July 2004)

A competition between a ferromagnetic metallic phase and a charge/orbital-ordered insulating one has been investigated for manganese oxides with perovskite structure, $RE_{1-x}AE_xMnO_3$ ($x=0.45$) with RE and AE being rare earth elements (more than 50 specimens mostly in forms of single crystal), ranging from La to Gd, and alkaline earth elements, Ca, Sr, and Ba, respectively. The global phase diagram is deduced in the plane of the effective one-electron bandwidth versus the magnitude of quenched disorder, which can be controlled by the averaged value and the variance of the RE/AE ionic radii, respectively. As the disorder increases, the long range orders of both phases tend to be suppressed, and the bicritical feature of the ferromagnetic metal versus the charge/orbital-ordered insulator is changed to such a complex one as intervened by a spin glasslike insulator that is viewed as the frozen state of charge/orbital correlation. The ferromagnetic transition temperature is critically suppressed near the phase boundary with the spin-glass, where the colossal magnetoresistance is most enhanced.

DOI: 10.1103/PhysRevB.70.014432 PACS number(s): 75.30.Kz, 71.27.+a, 71.30.+h

I. INTRODUCTION

The manganese oxides with perovskite structure, $RE_{1-x}AE_xMnO_3$ (RE and AE being rare earth and alkaline earth elements, respectively), have extensively been studied in the light of a close interplay among spin, charge, orbital, and lattice degrees of freedom.[1] For $RE_{1-x}AE_xMnO_3$, one of key parameters to determine what phase is realized is a transfer interaction of the e_g-state conduction electron between neighboring Mn sites [or the effective one-electron bandwidth (W) of the e_g-band]. The effective W is dependent on a lattice distortion of the perovskite structure, namely the tilting of MnO_6 octahedra (or the Mn-O-Mn bond angle), the degree of which can be finely changed by the averaged ionic radius of perovskite A site cations ($r_A=(1-x)r_{RE3+}+xr_{AE2+}$) in terms of tolerance factor.[2] Since the double exchange interaction being responsible for the ferromagnetic metal (FM) state[3–5] is scaled by the W,[6,7] the FM is relatively destabilized in a distorted perovskite manganite. In such a case, the FM is frequently replaced by competing phases against the FM, e.g., an antiferromagnetic insulator with charge/orbital ordering (CO/OO).[8–10]

As it has been argued by recent theoretical and experimental studies,[11–16] the stability of the FM as well as the CO/OO is affected also by the presence of quenched disorder, such as doped impurities (e.g., Cr^{3+}) on the Mn-sites, grain boundaries of polycrystalline ceramics, and random chemical substitution of RE with AE. In particular, the solid solution of RE and AE is a common technique to control the band filling (doping level) of the system in the perovskites and related oxide materials,[17] yet such a moderate disorder is known to cause a large modification in the transition temperature T_C of the FM phase[18,19] and even in the phase diagram itself.[15,20] The magnitude of the quenched disorder (perhaps the local structural variation) arising from such a solid solution can be evaluated by the variance of the ionic radii, $\sigma^2=\Sigma(x_i r_i^2-r_A^2)$, where x_i and r_i are the fractional occupancies and the effective ionic radii of cations of RE and AE, respectively, as demonstrated by Rodriguez-Martinez and Attfield.[18,19]

In this paper, we comprehensively describe the competing features between FM and CO/OO for $RE_{1-x}AE_xMnO_3$ ($x=0.45$) crystals. The reason why we have chosen the doping level of $x=0.45$ is that near the half-doping ($x=0.5$) the phase competition and the resultant phase variation are most clearly seen, but that the exact $x=0.5$ crystals are known to show the special stability of the CO/OO phase unique to the commensuration effect.[15,21,22] We demonstrate here the whole electronic phase diagram of $RE_{1-x}AE_xMnO_3$ ($x=0.45$) with the variation of both r_A (bandwidth) and σ^2 (magnitude of disorder).

II. EXPERIMENT

Most of the samples, except for the series of $(Pr_{1-y}La_y)_{0.55}Ca_{0.45}MnO_3$ ($0.2<y\leqslant 1$) and $La_{0.55}(Ca_{1-y}Sr_y)_{0.45}MnO_3$ ($0\leqslant y<1$), have been prepared as the single crystals by the floating zone method. The details of the crystal growth procedure have been described in Refs. 15 and 23. The obtained crystals were checked by the powder x-ray diffraction, which indicated that the crystal was single phase. Magnetization was measured by a SQUID magnetometer, and resistivity in magnetic fields (up to 7 T) was measured in a cryostat equipped with a superconducting magnet. For the ac susceptibility measurement, the amplitude was set at 10 Oe and the frequency was changed from 500 Hz to 10000 Hz.

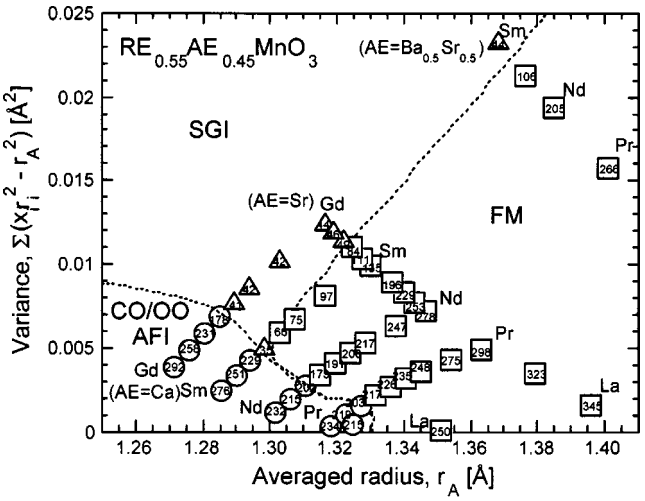

FIG. 1. The transition temperatures of T_C (squares), T_{CO} (circles), and T_G (triangles) for various $RE_{1-x}AE_xMnO_3$ ($x=0.45$) crystals plotted on the r_A and σ^2 plane. The phases of ferromagnetic metal, charge/orbital-ordered antiferromagnetic insulator, and spin glasslike insulator are denoted as FM, CO/OO AFI, and SGI, respectively.

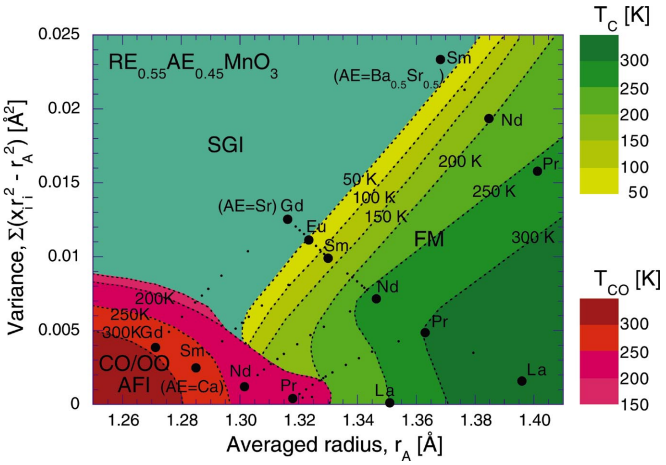

FIG. 2. (Color) The electronic phase diagram of various $RE_{1-x}AE_xMnO_3$ ($x=0.45$) crystals in the plane of r_A and σ^2. Abbreviations of FM, CO/OO AFI, and SGI are same as indicated in Fig. 1. Contour lines of the respective transition temperatures are drawn by extrapolation on the basis of the data shown in Fig. 1. Small and large dots (more than 50 points) indicate the materials that were actually synthesized, mostly in form of single crystal, and characterized.

III. RESULTS AND DISCUSSION

First, we show in Fig. 1 the experimental data of the transition temperatures for the FM, CO/OO, and spin glasslike insulator (SGI) (Ref. 24) phases in the $r_A-\sigma^2$ plane, as realized in $RE_{1-x}AE_xMnO_3$ ($x=0.45$) crystals synthesized and investigated in this study. In this figure, T_C and T_{CO} in cooling and warming runs are determined as the temperature at which $|d \ln \rho/d(1/T)|$ in the corresponding temperature profile of resistivity becomes maximum.[25] It has been experimentally confirmed for several $x=0.45$ crystals, e.g., $Pr_{0.55}(Ca_{1-y}Sr_y)_{0.45}MnO_3$ (Ref. 15) that this procedure can give the correct value of T_{CO} that is deduced by diffraction measurements. The values of T_C and T_{CO} dipicted in Fig. 1 are the averaged ones of the both cooling and warming runs. (For $La_{0.55}Ca_{0.45}MnO_3$, T_C has been cited from Ref. 26.) Accordingly, T_G is the temperature at which ac susceptibility (χ') taken at 500 Hz, or the zero-field-cooled (ZFC) magnetization at 100 Oe has a cusp structure. (The detailed temperature profiles of resistivity and magnetization as the evidence for the phase transformation will be exemplified in the following.) On the basis of these observations, we show in Fig. 2 the electronic phase diagram of $RE_{1-x}AE_xMnO_3$ ($x=0.45$) crystals plotted on the r_A-σ^2 plane. First, for the lower-left and lower-right regimes, where the σ^2 is relatively small, the CO/OO and the FM are dominant, respectively. In $RE_{0.55}Ca_{0.45}MnO_3$ (RE=Gd, Sm, Nd, and Pr), the CO/OO transition temperature T_{CO} shows a decrease from ~300 K to ~230 K as RE changes from Gd to Pr. In $RE_{0.55}Sr_{0.45}MnO_3$ (RE=La, Pr, Nd, Sm, and Gd), on the other hand, the T_C decreases from ~350 K to ~130 K as RE changes from La to Sm. These features for both of CO/OO and FM regions may be interpreted in terms of the change of W. Furthermore, as shown in the cases of $RE_{0.55}(Ca_{1-y}Sr_y)_{0.45}MnO_3$ (RE=Sm, Nd, and Pr) ($0 \leqslant y \leqslant 1$), the CO/OO is replaced with the FM with increase in y, which may also be explained by the increase in W. Thus, the keen competition between the CO/OO and FM forms a prototypical bicritical point.[15] It is noted, however, that for the upper regime in this figure the SGI becomes dominant.[23] In $RE_{0.55}(Ca_{1-y}Sr_y)_{0.45}MnO_3$ (RE=Gd) ($0 \leqslant y \leqslant 1$), for example, the CO/OO is replaced with the SGI for $y>0.3$.

As the examples of experimental data that have been used to deduce the global phase diagram (Fig. 2), we show in Fig. 3 the temperature profiles of resistivity (a-c) and the electronic phase diagrams (d-f) for $RE_{0.55}(Ca_{1-y}Sr_y)_{0.45}MnO_3$ ($0 \leqslant y \leqslant 1$) with RE=Gd [(a) and (d)], Sm [(b) and (e)], and Nd [(c) and (f)], respectively. In Figs. 3(a) and 3(b), the resistivities for $y=0$ show anomalies around 295 K (for RE=Gd) and 275 K (for RE=Sm) in both cooling and warming runs, respectively, which manifests the CO/OO transition. In common to the both cases, the T_{CO} is lowered, and the transition becomes broadened upon the moderate substitution of Ca with Sr. In the case of RE=Gd, no distinct change is discerned in temperature profiles of resistivity for $y \geqslant 0.4$. For $y=1$, the x-ray diffuse scattering around (2 3/2 0) of the orthorhombic *Pbnm* setting is seen below about 250 K, which is indicative of the short range CO/OO correlation.[23] In the case of RE=Sm, on the other hand, the CO/OO transition is still discerned at around 170 K at $y=0.35$, while it is abruptly replaced with the FM for $y \geqslant 0.5$.

The inset of Fig. 3(d) shows temperature profiles of ac susceptibility for the $y=0.4$ crystal of $Gd_{0.55}(Ca_{1-y}Sr_y)_{0.45}MnO_3$. The susceptibility becomes frequency dependent below about 40 K, that is, the SGI becomes prevailing below about 40 K for this crystal. Similarly, the inset of Fig. 3(e) shows temperature profiles of ZFC and FC magnetization for the $y=0.35$ crystal of $Sm_{0.55}(Ca_{1-y}Sr_y)_{0.45}MnO_3$. The magnetization shows a tiny decrease around 180 K and a cusp structure around 120 K.

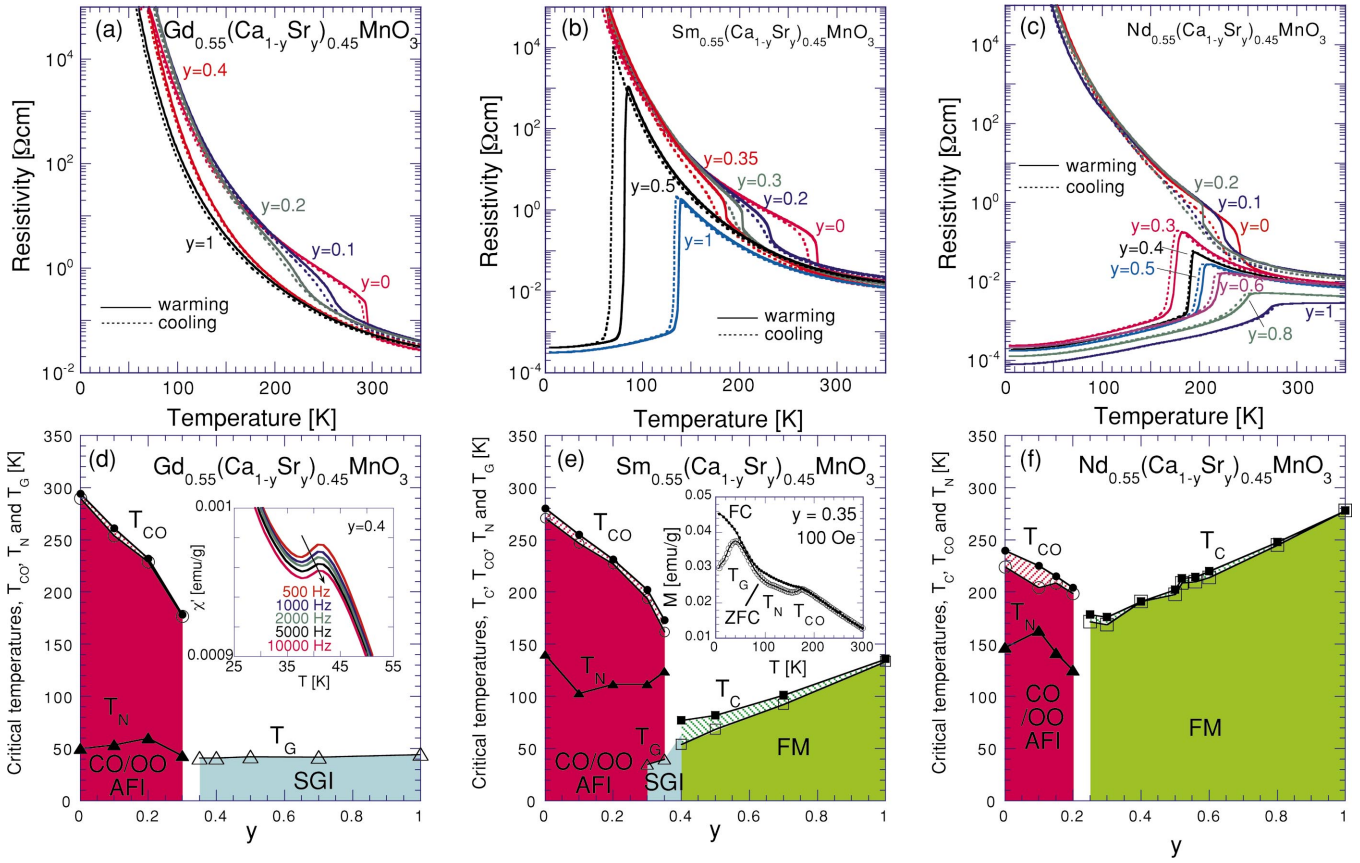

FIG. 3. (Color) Temperature profiles of resistivity (a-c) and the electronic phase diagrams (d-f) for $RE_{0.55}(Ca_{1-y}Sr_y)_{0.45}MnO_3$ ($0 \leqslant y \leqslant 1$) with RE=Gd [(a) and (d)], Sm [(b) and (e)], and Nd [(c) and (f)]. The T_{CO} and T_C, which were determined by the resistivity measurement, are indicated by circles and squares, respectively. The temperatures in the cooling and warming runs are denoted as open and closed symbols, respectively. The hysteresis regions are hatched. The Neel temperature T_N is denoted as closed triangles. The spin glass (SG) transition temperature T_G is indicated by open triangles. The abbreviations, FM, CO/OO AFI, and SGI, are the same in Fig. 1. Insets show temperature profiles of ac susceptibility (χ') for the $y=0.4$ crystal of $Gd_{0.55}(Ca_{1-y}Sr_y)_{0.45}MnO_3$ (d), and zero-field-cooled (ZFC) as well as field-cooled (FC) magnetization (M) for the $y=0.35$ crystal of $Sm_{0.55}(Ca_{1-y}Sr_y)_{0.45}MnO_3$ (e).

With further decrease in temperature, discrepancy between the ZFC and FC magnetization is pronounced below ~40 K, which is also indicative of the reentrant SGI below ~40 K. Incidentally, such a discrepancy between the ZFC and FC magnetization is observed also for the SGI phase of the $y=0.4$ crystal, while the frequency dependence of the ac susceptibility also for that of the $y=0.35$ crystal.

The electronic phase diagrams for $Gd_{0.55}(Ca_{1-y}Sr_y)_{0.45}MnO_3$ and $Sm_{0.55}(Ca_{1-y}Sr_y)_{0.45}MnO_3$ ($0 \leqslant y \leqslant 1$) are summarized in Figs. 3(d) and 3(e), respectively. In the case of RE=Gd, even when W is increased by substitution of Ca with Sr, the CO/OO is replaced with the SGI for $y \geqslant 0.35$, not with the FM. In the case of RE=Sm, the CO/OO is kept at $0 \leqslant y \leqslant 0.3$, while it changes to the FM at $y \geqslant 0.4$. In the narrow intermediate regime of $0.3 \leqslant y \leqslant 0.4$, however, the SGI appears reentrantly below about 40 K in spite of that the CO/OO transition is seen at a higher temperature.

Figures 3(c) and 3(f) show the temperature profiles of resistivity and electronic phase diagram for $Nd_{0.55}(Ca_{1-y}Sr_y)_{0.45}MnO_3$, respectively. In Fig. 3(c), the CO/OO at $y=0$ is manifested by the resistivity anomaly around 235 K. As y increases up to 0.2, the T_{CO} is lowered to about 200 K, and with further increase in y, the FM emerges at $y=0.25$ with $T_C \sim 165$ K. As a result, as shown in Fig. 2(f), the T_{CO} and T_C are comparable at $y=0.2-0.25$, indicating a prototypical bicritical feature, which is similar to that reported for $Pr_{0.55}(Ca_{1-y}Sr_y)_{0.45}MnO_3$.[15]

Figure 4 shows critical temperatures as a function of r_A for the typical two cases; one (bottom panel) is for the relatively small disorder in moving from $Gd_{0.55}Ca_{0.45}MnO_3$ to $La_{0.55}Sr_{0.45}MnO_3$, i.e., $RE_{0.55}Ca_{0.45}MnO_3$ with varying RE from Gd to Pr, $Pr_{0.55}(Ca_{1-y}Sr_y)_{0.45}MnO_3$ with varying y from 0 to 1, and then $(Pr_{1-y}La_y)_{0.55}Sr_{0.45}MnO_3$ with varying y from 0 to 1. The other (top panel) is for the relatively large disorder ranging from $Gd_{0.55}(Ca_{1-y}Sr_y)_{0.45}MnO_3$ with varying y from 0 to 1, and $RE_{0.55}Sr_{0.45}MnO_3$ with varying RE from Gd to Pr, and La. The both scanning routes of materials are indicated by thick lines in the middle panel (global phase diagram) of Fig. 4. In the case with the relatively small disorder, a typical bicritical feature is seen with $T_{CO} \sim T_C \sim 200$ K, which occurs at $y \sim 0.2$ in $Pr_{0.55}(Ca_{1-y}Sr_y)_{0.45}MnO_3$.[15] In the case with the relatively large disorder, the T_{CO} decreases and the CO/OO turns into to a SGI as y increases in $Gd_{0.55}(Ca_{1-y}Sr_y)_{0.45}MnO_3$. Even in $RE_{0.55}Sr_{0.45}MnO_3$, the SGI remains for RE=$(Gd_{1-y}Sm_y)$ with

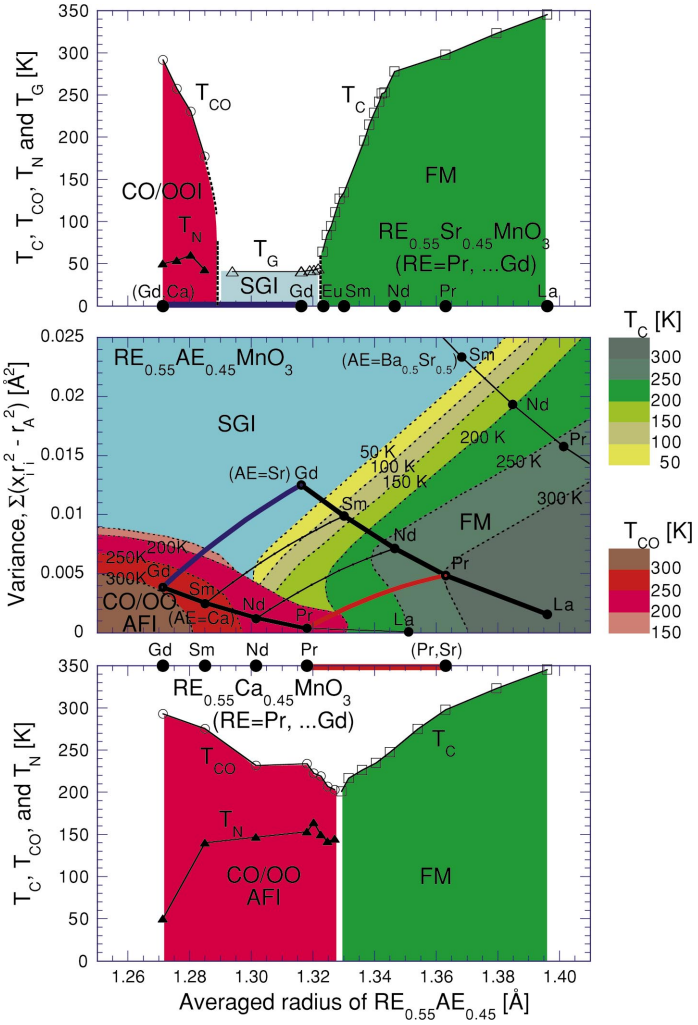

FIG. 4. (Color) Critical temperatures as a function of r_A for the cases with relatively small (bottom panel) and large (top panel) disorder, respectively. The middle panel reproduces the phase diagram plotted on the r_A-σ^2 plane, in which the traces of the two cases are drawn. For the relatively small disorder, the critical temperatures are plotted in going from $Gd_{0.55}Ca_{0.45}MnO_3$ to $La_{0.55}Sr_{0.45}MnO_3$, through $RE_{0.55}Ca_{0.45}MnO_3$ varying RE from Gd to Pr, $Pr_{0.55}(Ca_{1-y}Sr_y)_{0.45}MnO_3$ varying y from 0 to 1, and $(Pr_{1-y}La_y)_{0.55}Sr_{0.45}MnO_3$ varying y from 0 to 1. For the relatively large disorder, those are plotted for the materials scans for $Gd_{0.55}(Ca_{1-y}Sr_y)_{0.45}MnO_3$ with varying y from 0 to 1, and for $RE_{0.55}Sr_{0.45}MnO_3$ with varying RE from Gd to Pr, and La. For the both cases, the T_{CO} and T_C are the averaged values in the cooling and warming runs, which are indicated by open circles and squares, respectively. The Neel temperature T_N and the spin-glass transition temperature T_G are denoted as closed and open triangles, respectively. The abbreviations, FM, CO/OO AFI, and SGI, are the same in Fig. 1.

$0 \leqslant y \leqslant 0.5$, while it is replaced with the FM with $y > 0.5$. As a result, Fig. 4 demonstrates that the bicritical feature as seen for the relatively small disorder is modified to a rather complex one including the SGI phase for the relatively large disorder even though the r_A (and hence the averaged lattice structure) is used as a common parameter on the abscissa. This feature has also been predicted by the simulation for the model system of manganites.[13]

Finally, Fig. 5 focuses on the region with the large W and σ^2, i.e., the upper–right region of the global phase diagram (Fig. 1), showing temperature profiles of resistivity for $RE_{0.55}(Ba_{0.5}Sr_{0.5})_{0.45}MnO_3$ (RE=La, Pr, Nd, $Nd_{0.5}Sm_{0.5}$, and Sm). In Fig. 5, the T_C decreases from ~360 K to ~110 K with varying RE from La to $Nd_{0.5}Sm_{0.5}$, and the FM is no more seen at RE=Sm. The inset shows ac susceptibility for RE=Sm. The susceptibility becomes frequency dependent below about 48 K, indicating that the ground state for RE=Sm is a SGI. Figure 5 again shows that the SGI is stabilized as disorder increases even when the W is large.[20] The magnetic field dependence of resistivity curves for $(Nd_{0.5}Sm_{0.5})_{0.55}(Ba_{0.5}Sr_{0.5})_{0.45}MnO_3$ is also shown in Fig. 5. Again the colossal magnetoresistance phenomena are ubiq-

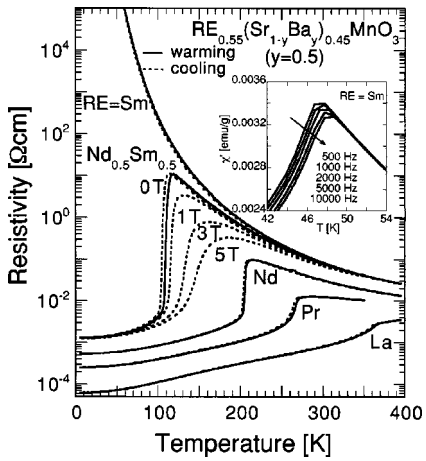

FIG. 5. (Color online) Temperature profiles of resistivity for $RE_{0.55}(Ba_{0.5}Sr_{0.5})_{0.45}MnO_3$ (RE=La, Pr, $Nd_{0.5}Sm_{0.5}$, and Sm). For $RE=Nd_{0.5}Sm_{0.5}$, the resistivity in magnetic fields is also shown. Inset shows the ac susceptibility (χ') at low temperatures for RE=Sm.

uitous around T_C of the FM locating close to the phase boundary with the SGI.

IV. SUMMARY

In summary, we have demonstrated the whole phase diagram of the colossal magnetoresistive (CMR) manganites of $RE_{1-x}AE_xMnO_3$ ($x=0.45$) with the variation of the effective one-electron bandwidth and the quenched disorder, which are experimentally controlled by the averaged ionic radius and the variance of the ionic radii upon the solid solution of rare-earth (RE^{3+}) and alkaline earth (AE^{2+}) ions. The Y–shaped bicritical feaure of the phase diagram due to the competition between the ferromagnetic metal and the antiferromagnetic charge/orbital ordered insulator is modified to the complex one intervened by a spin glass insulator with increasing the quenched disorder. Under a relatively large disorder, therefore, neither of the long-range ordered states, the ferromagnetic metal nor the charge/orbital-ordered insulator, emerges, and a spin glasslike insulator dominates the whole phase diagram. Near the phase boundary with such a disorder–induced spin-glass insulator, the T_C of the ferromagnetic metal is critically suppressed and the colossal magnetoresistance effect is most enhanced.

ACKNOWLEDGMENT

The authors would like to thank N. Nagaosa for enlightening discussions.

[1] Y. Tokura and N. Nagaosa, Science **288**, 462 (2000).
[2] J. B. Torrance, P. Lacorre, A. I. Nazzal, E. J. Ansaldo, and Ch. Niedermayer, Phys. Rev. B **45**, 8209 (1992).
[3] C. Zener, Phys. Rev. **82**, 403 (1951).
[4] P. W. Anderson and H. Hasegawa, Phys. Rev. **100**, 675 (1955).
[5] P.-G. de Gennes, Phys. Rev. **118**, 141 (1960).
[6] N. Furukawa, J. Phys. Soc. Jpn. **64**, 2734 (1995).
[7] N. Furukawa, J. Phys. Soc. Jpn. **64**, 2754 (1995).
[8] Z. Jirak, S. Krupicka, Z. Simsa, M. Dlouha, and Z. Vratislav, J. Magn. Magn. Mater. **53**, 153 (1985).
[9] E. Pollert, S. Krupicka, and E. Kuzmicova, J. Phys. Chem. Solids **43**, 1137 (1982).
[10] Z. Jirak, S. Krupicka, V. Nekvasil, E. Pollert, G. Villeneuve, and F. Zounova, J. Magn. Magn. Mater. **15-18**, 519 (1980).
[11] A. Moreo, M. Mayr, A. Feiguin, S. Yunoki, and E. Dagotto, Phys. Rev. Lett. **84**, 5568 (2000).
[12] M. Uehara, S. Mori, C. H. Chen, and S.-W. Cheong, Nature (London) **399**, 560 (1999).
[13] J. Burgy, M. Mayr, V. Martin-Mayor, A. Moreo, and E. Dagotto, Phys. Rev. Lett. **87**, 277202 (2001).
[14] J. Burgy, A. Moreo, and E. Dagotto, Phys. Rev. Lett. **92**, 097202 (2004).
[15] Y. Tomioka and Y. Tokura, Phys. Rev. B **66**, 104416 (2002).
[16] Y. Motome, N. Furukawa, and N. Nagaosa, Phys. Rev. Lett. **91**, 167204 (2003).
[17] M. Imada, A. Fujimori, and Y. Tokura, Rev. Mod. Phys. **70**, 1039 (1998).
[18] L. M. Rodriguez-Martinez and J. P. Attfield, Phys. Rev. B **54**, R15622 (1998).
[19] L. M. Rodriguez-Martinez and J. P. Attfield, Phys. Rev. B **63**, 024424 (2000).
[20] D. Akahoshi, M. Uchida, Y. Tomioka, T. Arima, Y. Matsui, and Y. Tokura, Phys. Rev. Lett. **90**, 177203 (2003).
[21] Y. Tokura, H. Kuwahara, Y. Moritomo, Y. Tomioka, and A. Asamitsu, Phys. Rev. Lett. **76**, 3184 (1996).
[22] H. Kuwahara, Y. Moritomo, Y. Tomioka, A. Asamitsu, M. Kasai, R. Kumai, and Y. Tokura, Phys. Rev. B **56**, 9386 (1997).
[23] Y. Tomioka, Y. Okimoto, J. H. Jung, R. Kumai, and Y. Tokura, Phys. Rev. B **68**, 094417 (2003).
[24] T. Terai, T. Sasaki, T. Kakeshita, T. Fukuda, T. Saburi, H. Kitagawa, K. Kindo, and M. Honda, Phys. Rev. B **61**, 3488 (2000).
[25] S-W. Cheong, H. Y. Hwang, C. H. Chen, B. Batlogg, L. W. Rupp, Jr., and S. A. Carter, Phys. Rev. B **49**, 7088 (1994).
[26] S-W. Cheong and H. Y. Hwang, in *Colossal Magnetoresistive Oxide*, edited by Y. Tokura (Gordon and Breach, Amsterdam, 2000), p. 237.